Quantum Reorientational Excitations in the Raman Spectrum of Hydrogen

Philip Dalladay-Simpson,^{1,*} Eric Edmund,¹ Huixin Hu,¹ Mario Santoro,^{2,3,†} and Federico Aiace Gorelli^{1,2,3,4,‡}

¹Center for High Pressure Science and Technology Advanced Research, 1690 Cailun Road, Shanghai, 201203, China
²Istituto Nazionale di Ottica, Consiglio Nazionale delle Ricerche (CNR-INO), via N. Carrara 1, 50019 Sesto Fiorentino, Italy

³European Laboratory for Non Linear Spectroscopy (LENS), via N. Carrara 1, 50019 Sesto Fiorentino, Italy

⁴Shanghai Advanced Research in Physical Sciences (SHARPS), Shanghai, China

Low-frequency Raman peaks, below 250 cm⁻¹, are observed in hydrogen between 2–174 GPa and 13–300 K. The origin of these features is attributed to reorientational transitions ($\Delta J = 0$; Q_0 -branch), which shift from the Rayleigh line as anisotropic intermolecular interactions lift the m_J degeneracy. This family of excitations closely follows the behavior of the S_0 -branches, sharing their dependence on pressure, temperature, and ortho- H_2 concentration. Above 65 K, spectra corrected by the Bose-Einstein population factor reveal a broad continuum arising from populated higher J-states and increased ortho-para disorder. Upon entering phase III, where molecular rotation is inhibited, this continuum is quenched, giving way to well-established optical phonons. Below 25 K, equilibrated samples demonstrate a fine structure from isolated and pair excitations from impurity ortho- H_2 molecules in a parahydrogen lattice, the latter a sensitive probe to anisotropic intermolecular interactions relevant to the quantum modeling of solid H_2 .

Hydrogen is a prototypical quantum solid, evidenced by its inflated volume due to large zero-point motion, the preservation of its rotational dynamics to 0 K and the existence of nuclear spin isomers [1-3]. The latter is a consequence of the total nuclear spin state of the molecule, I, and the rotational quantum number, J, being coupled and results in two distinct molecular species of hydrogen: para-H₂ $(I = 0; \text{ singlet-state: } \frac{1}{\sqrt{2}}(|\uparrow\downarrow\rangle - |\downarrow\uparrow\rangle) \text{ only}$ occupying even-J rotational levels and ortho- H_2 (I=1; triplet-state: $|\uparrow\uparrow\rangle$, $|\downarrow\downarrow\rangle$ and $\frac{1}{\sqrt{2}}(|\uparrow\downarrow\rangle+|\downarrow\uparrow\rangle)$ only occupying odd-J levels [4]. Raman spectroscopy has been foundational in probing this quantum nature since its inception almost a century ago, providing early validation of quantum mechanics [4, 5] through the characterization of the relative intensities of the rotational $S_1(J)$ -branch, a direct signature of spin isomers and their thermal equilibrium concentration (1:3, para:ortho) at room temperature [6].

Raman spectroscopy remains pivotal, having mapped out most of hydrogen's condensed phases prior to its longsought density-driven metallization [7]. This includes the discovery of the broken-symmetry phase (Phase II)[8], the orientationally ordered phase (Phase III) [9], and the layered mixed-molecular phases (Phases IV/V) [10–12], providing key constraints for the most advanced quantum models of hydrogen [13–15]. Up to 150 GPa, hydrogen's phase diagram is dominated by phase I, which is characterized by a hexagonal close-packed (hcp) lattice of coupled quantum rotors [1–3]. In phase I, increased intermolecular interactions reduce J as an effective quantum number [16, 17]. However, where J remains a good quantum number, below ~70 GPa [16], the Raman spectrum of phase I is remarkably simple and characterized by vibrational $(\nu_{1\to 0})$, rotational $(S_0(J); \Delta J=2)$, and E_{2g} phonon modes. Notably, with the lowest rotational excitation $S_0(0)$ at 350 cm⁻¹ and the lowest E_{2q} phonon frequency recorded being 37 cm⁻¹ [18], one might expect

a spectral gap below which no Raman excitations are observable.

Anisotropic interactions in hydrogen lift the 2J + 1degeneracy of the orientational sub-levels, m_{J} , giving rise to low-energy Raman-active reorientational excitations where the J number is preserved, ie. a Q-branch. These were first identified over 50 years ago by pioneering Raman spectroscopy measurements on solid hydrogen at ambient pressure and low temperatures [18]. Subsequent studies, under similar conditions, detected them in a dilute-ortho-H₂ solid via microwave absorption [19] and, later, as combination bands with infrared absorption [20]. The excitations are characteristically very low in Raman frequency, less than 6 cm⁻¹ [21], making them particularly challenging to observe given their proximity to the Rayleigh line. However, high pressure is expected to amplify the underlying anisotropic interactions, thereby increasing their associated frequencies and intensities into more readily experimentally accessible regimes. Recent simulations have suggested that this reorientational branch exhibits a fine structure at room temperature with components reaching frequencies $\sim 7-70 \text{ cm}^{-1}$ at 40 GPa [22]. However, because of their symmetry, they are not observable in a perfectly back-scattering geometry with the c-axis parallel to the collection direction [17, 22]. Therefore, due to the crystallographic preferred orientation of hydrogen in a Diamond Anvil Cell (DAC) [23, 24] this has remained an experimental blind spot for high-pressure studies. As a consequence, their only tentative identification in D₂ required a 90° scattering geometry [18], a technical limitation for high-pressure experiments.

In this study low-frequency Raman peaks, below 250 cm^{-1} , have been observed between 2-174 GPa and 13-300 K. We interpret the origin of these features as reorientational transitions, a Q_0 -branch, between orientational sub-levels (m_J) within the same rotational state

J of the ground vibrational manifold. The appearance of these transitions is due to the lifting of m_J degeneracy, caused by anisotropic nearest neighbor (nn) interactions in the crystalline lattice, without which they would occur at zero-frequency. The Bose-Einstein population (BEP) corrected spectral line shape is found to be highly dependent on temperature and ortho-H₂ concentration. At higher temperatures, above 65 K, a lowfrequency broad Boltzmann-like distribution is observed, consistent with a thermal population of higher J-states and increased ortho-para nn configurational disorder. These excitation's behavior is similar to that of the rotational S_0 -branches, further supporting the interpretation that both arise from quantum orientational motion. Upon entering phase III, where molecular rotation is arrested, this broad distribution quenches into the wellresolved, known phonons of that phase [25, 26]. In phase I at low temperatures, below 25 K, and dilute orthoconcentrations, less than 5 %, a resolved fine structure emerges, indicative of impurity pair and isolated ortho- H_2 excitations [1, 2, 19]. This pressure-dependent fine structure serves as a sensitive probe of the anisotropic intermolecular interactions essential for constraining models of solid hydrogen.

Figs. 1(a, c), 2 and End Matter Fig. 5(a, b) present raw measurements on samples of hydrogen in phase I at various pressures and down to 17 K, these spectra reveal the expected rotational S_0 -branches of a quantum rotor and the weaker optical E_{2g} phonon of the hcp lattice. Across all spectra above 2.4 GPa, we observe a prominent and previously unaccounted-for feature characterized by a strong increase in intensity toward zero frequency in both the Stokes and anti-Stokes regions. As a result, this unusual lineshape appears almost like a peak centered at zero frequency, which is non-physical for a Raman excitation. As a consequence, this feature could easily be mistaken for an experimental artifact, such as poor filtration of the Raman excitation source and/or sample/diamond photoluminescence and perhaps explains why it has been disregarded in previous studies [17, 27].

For low-frequency excitations at finite temperatures, the Raman lineshape is significantly influenced by the Bose-Einstein population factor, which can result in distorted profiles [28, 29]. To recover the bare Raman cross-section, we applied a temperature-fitted BEP correction, dividing the Stokes and anti-Stokes intensities by $(1 + n(\omega, T))$ and $n(\omega, T)$, respectively, where $n(\omega, T)$ is the Bose-Einstein factor (See End Matter for details). The resulting BEP-corrected spectrum, which is symmetric around zero-frequency, is shown by the blue trace in Figs. 1(a, c) and Fig. 5(a) as well as the waterfall of spectra in Figs. 1(b, c), 3, 5(b, c) and 6. This correction successfully resolves the strong peak centered around the Rayleigh line into a weaker but distinct low-energy Stokes/anti-Stokes pair of excitations, with Boltzmannlike distributions up to $250~\mathrm{cm}^{-1}$. The validity of this

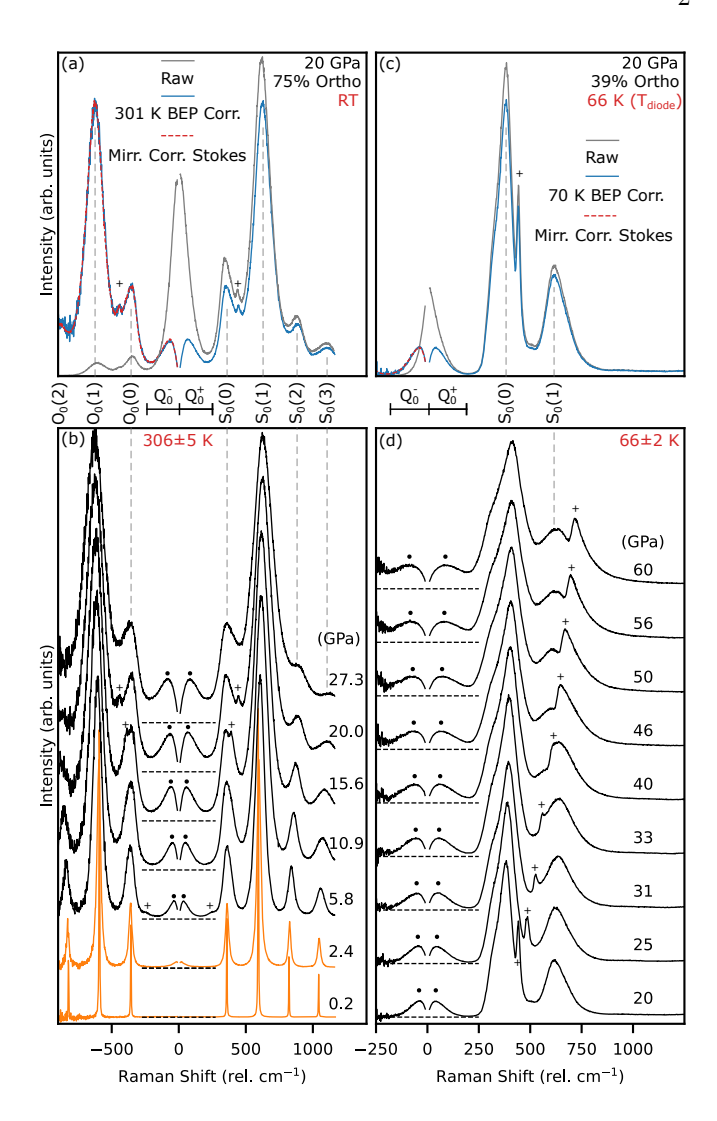


FIG. 1. 532 nm excited Raman spectroscopy of H₂ during isothermal compressions; (1) left panels (a,b), room temperature from 0.2-27.3 GPa and (2) right panels (c,d) at 66 K from 20-60 GPa. Fluid H₂ and solid H₂ are plotted with orange and black traces respectively. Top panels (a) and (c) present a raw Raman spectrum at 20 GPa (gray), the BEP corrected spectrum (blue) and the mirrored corrected Stokes spectrum (dashed red). Bottom panels (b) and (d), are waterfall plots of the corrected spectra, with the average temperature and its error bar (one standard deviation (SD)) determined spectroscopically from the BEP correction. Dashed horizontal lines mark the zero-intensity baselines for each spectrum. Dots and crosses denote the maxima of the Q_0 -branches and the frequency of the E_{2g} phonon peak, respectively. The rotational excitations are highlighted as $S_0(J)$ and $O_0(J)$, for Stokes and anti-Stokes, respectively.

procedure is confirmed by the excellent agreement between the anti-Stokes side of the BEP-corrected spectrum and the mirrored corrected Stokes side, as shown by the red dashed traces in Figs. 1(a, c) and 5(a). This agreement unambiguously validates the signal as symmetric, first-order Raman activity around the Rayleigh line as

seen in Figs. 1, 5 and 6. It is also further substantiated by being observed with both 532 and 660 nm Raman excitation wavelengths, shown in Figs. 1 and 5, respectively. Interestingly, despite hydrogen's transparency to visible light, a marginal laser heating effect is evident in all measurements, with fitted spectral temperatures up to 10 K higher than those measured on the DAC body.

Given the low frequency of these excitations, with the tail of the distribution approaching zero-frequency and therefore zero energy, we assign it to a family of lowenergy reorientational transitions [1, 18, 21]. These excitations, generated by transitions between the m_J orientational sub-levels, occur within the vibrational ground state and preserve the initial rotational quantum number J (for J > 0). For an isolated molecule, the m_J sub-levels are 2J+1-fold degenerate, but in a condensed state, anisotropic intermolecular interactions partially split them, shifting the transition energy away from zero [1, 2, 18, 19, 21]. From this point forward, we will refer to these quantum reorientational excitations as a Q_0 branch $(Q_0^+$ for Stokes, Q_0^- for anti-Stokes), the spectroscopic notation assigned due to the preservation of Jstate for the Raman transition. As mentioned previously, these branches were recently predicted to contribute to the Raman spectrum at high pressure [22], but was suggested to be unmeasurable in a back-scattering geometry [17, 22]. We attribute our successful observation to the high numerical aperture (NA) of the objective used, partially mitigating the orientational dependence of these excitations [17, 22]. Given at ambient pressure and low temperature a fine structure is characteristic for these excitations, as reported in both microwave absorption and infrared absorption measurements [19, 20]. We suggest that at elevated temperature, the fine-structure associated with orientational transitions is smeared out by ortho-para nn configurational disorder and thermal population of higher J-states, a phenomenon which is well-established for the rotational S_0 -branches [1, 30].

The behavior of this peak under pressure and temperature closely mirrors that of the S_0 rotational branches, as observed in both the BEP-corrected and uncorrected spectra (Figs. 1(b), 1(d), and 5). As seen in Fig. 1(b), the S_0 -branches are distinctly sharp in the low-density fluid state at 0.2 GPa, <5 cm⁻¹ FWHM, and as a result the Q_0 -branch is not resolved from the Rayleigh line. However, above 2.4 GPa, whilst still in a fluidstate, a small peak is found to emerge as the rotational S_0 -branches are broadened, $\sim 30 \text{ cm}^{-1}$ FWHM. This behavior continues into solid phase I, where both the S_0 and Q_0 -branches exhibit a moderate pressure dependence in frequency, unlike the E_{2g} phonon, but undergo significant pressure-induced broadening increasing by more than one order of magnitude over the investigated pressure range. This broadening is attributed to enhanced anisotropic interactions at higher pressures, which further lift the m_J degeneracy, alongside the hindering of rotations that reduce J as an effective quantum number [16, 17, 22].

At temperatures below 65 K, hydrogen consists almost entirely of the ground para- H_2 (J=0) and ortho- H_2 (J=1) states with the equilibrium ortho-H₂ concentration varying from $40 \rightarrow 0\%$ as temperature approaches 0 K. Figs. 1 and 2 demonstrate that as the thermal population of the J=1 state decreases, the intensities of the $S_0(1)$ and Q_0 bands diminish. This relationship is more clearly observed during the ortho-para conversion process shown in Fig. 2, which reveals a strong temporal correlation between the integral intensities of the Q_0 and $S_0(1)$ branches at 17 K and 29 GPa. The inset to Fig. 2(b), shows that the Q_0 and $S_0(1)$ -branch intensities decrease by factors of approximately 5 and 2.5, respectively, over 836 minutes as the system approaches its equilibrium ortho-para concentration. Meanwhile, we see an appreciable 40% gain in intensity of the $S_0(0)$ -branch resulting from an increased population of the J=0 state. This demonstrates that below 65 K, the Q_0 branch arises entirely from ortho-H₂ reorientational transitions within the J=1 manifold with no contribution from para-H₂ as its J=0 ground state is not degenerate.

The behavioral similarities between the rotational S_0 branches and the reorientational Q_0 -branches persist into phases II and III, structures defined by their quantum and classical orientational ordering, respectively [31]. The transition to phase II at 69 K at 100 GPa, is characterized by the disappearance of distinct spectral features, which are replaced by a broad continuum of Raman intensity extending up to 1200 cm^{-1} . As shown in End Matter Fig. 6, the minimum between the Q_0 and the S_0 -branches near 200 cm⁻¹ vanishes between 91 and 112 GPa. Interestingly, the lack of spectral structure is typically an indicator of a highly disordered state, which in turn presents a paradox, given that this phase has long been proposed to exhibit quantum orientational ordering of the molecular angular momenta[3, 31]. At higher pressures, >150 GPa and 69 K, the former $S_0(J)$ rotational bands are quenched, transforming into the optical phonons that mark the onset of phase III [25, 26], where molecular rotation is inhibited [3]. A parallel modification also occurs in the Q_0 -branches, whose broad continuum collapses into two distinct optical phonons below 200 cm⁻¹ which are also characteristic of phase III [26]. By correlating excitations across all three phases [31], this observed progression could provide crucial insight for constraining structural models of the currently structurally ambiguous phases of hydrogen, phases II and III [23, 24].

In our measurements at 17 K and 29 GPa, the ortho- $\rm H_2$ concentration was reduced to approximately 5% (See End Matter for determination of ortho-para concentration)[32], effectively rendering ortho- $\rm H_2$ to an impurity level within a bulk para- $\rm H_2$ crystal. This high-purity environment is evidenced by the better resolved

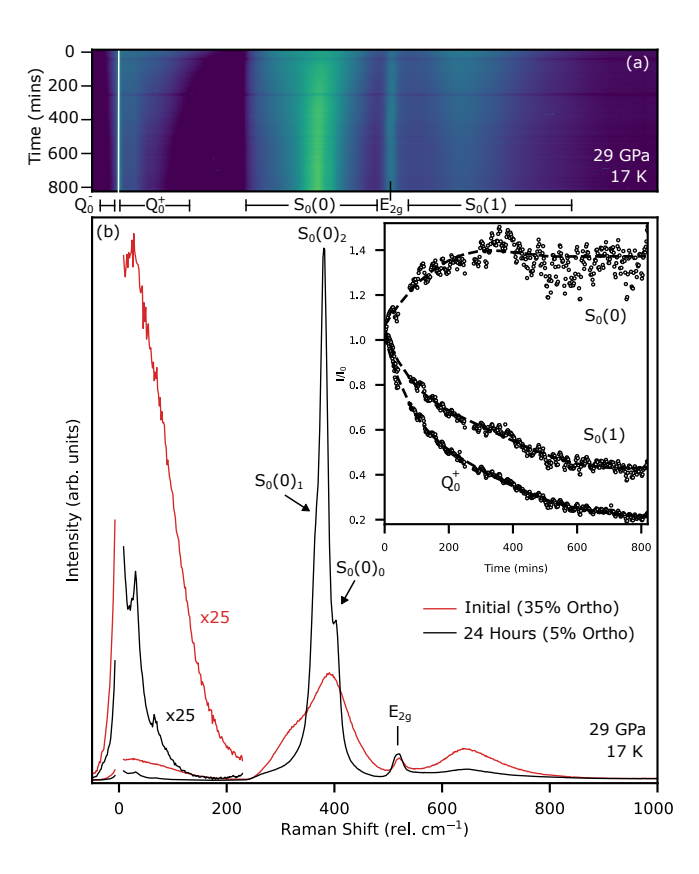


FIG. 2. (a) Raman logarithmic intensity heat map as a function of time measured at 17 K and 29 GPa. (b) Raw Raman measurements, normalized to the unstressed diamond edge, taken upon reaching the base temperature (red trace) and 24 hours later (black trace). (b) Inset shows the normalized integrated intensity over time for the Q_0^+ , $S_0(0)$ and $S_0(1)$ branches shown in panels (a,b).

orientational fine structure of the $S_0(0)$ peak, as seen by comparing the initial (2 hours at 17 K) and final spectra (24 hours at 17 K) in Fig. 2(b). This peak exhibits the characteristic triplet components— $S_0(0)_{|m|}$ for |m| = 0, 1, and 2—arising from the partially lifted degeneracy of the J=2 rotational level [30]. Concurrently with the resolution of the $S_0(0)$ triplet, relatively weak but distinct excitations emerge within the formerly broad Q_0 -branch below 100 cm⁻¹. In a subsequent, higher-purity sample (2% ortho-H₂) produced by maintaining the sample at 4.4 K for more than 60 hours, these excitations become even more pronounced as seen in Fig. 3, revealing at least seven partially resolved components below 100 cm^{-1} , which we label P_{1-7} , and were observed to be almost three orders of magnitude weaker than the most prominent $S_0(0)_2$ -excitation.

The pressure evolution of the Q_0 fine-structure frequencies, shown in Fig. 4, provides critical insight into their assignment and origin. The number of observed components and their splitting are consistent with the expected behavior for the J=1 manifold, where the sub-level structure depends strongly on the number of

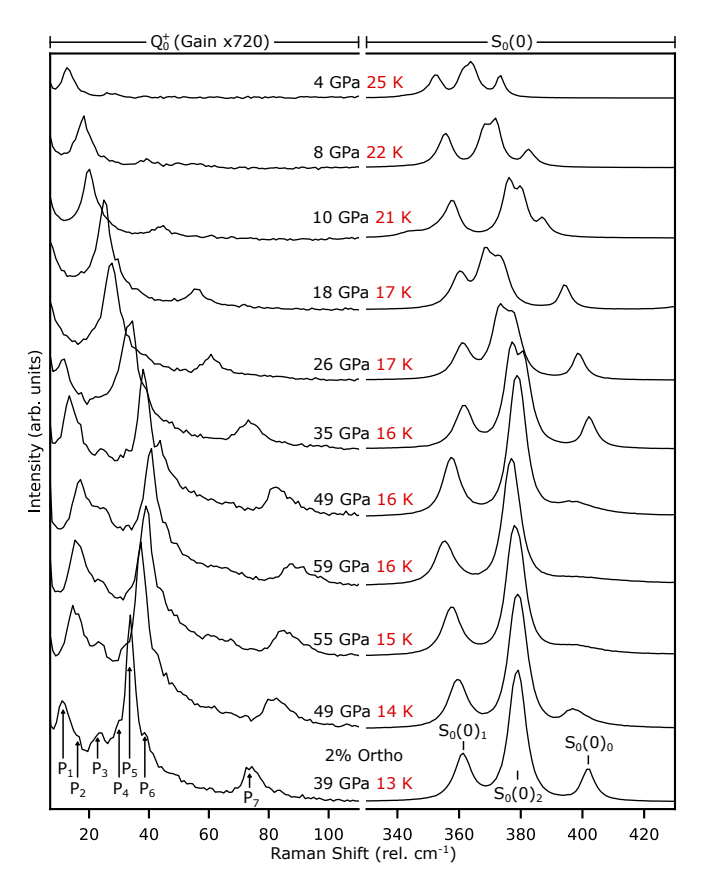


FIG. 3. Selected BEP corrected Raman spectra, excited by a 532 nm laser, of the Q_0 -branch and the $S_0(0)$ -branch for a compression (39-59 GPa) followed by decompression (59-4 GPa) of a 2% ortho-H₂ concentration sample. Measurements were performed over the course of several hours while the temperature as temperature increased from $13\rightarrow25$ K due to the exhaustion of L-He.

nn ortho- H_2 molecules surrounding a given ortho- H_2 molecule (nn_{ortho}) . For instance, for $nn_{ortho} = 0$ we should only observe two split reorientational sublevels, while if $nn_{ortho} = 1$ the total angular momentum quantum number of the pair will be 0, 1, or 2 leading up to 9 split reorientational sub-levels [1, 19, 21]. Where $nn_{ortho} > 1$ the picture rapidly becomes more complex, partially contributing to the broad distribution we find at higher-temperature higher-ortho-H₂ concentrations, befor expecting to finally simplify for a pure ortho-H₂ lattice. In our sample, assuming a perfect random distribution of ortho-H₂ molecular impurities (2% conc.), the resulting fractions are 78% isolated $(nn_{ortho} = 0)$, 19% existing as pairs $(nn_{ortho} = 1)$, and the remaining 3% in higher-order configurations (e.g., triplets or quadruplets) (for calculation details see equation (1) in ref. [33]).

The general hardening of these peaks with pressure, as shown in Fig. 4, highlights the increasing intermolecular anisotropic interactions. A global fit (see End Matter for details) to the pressure dependence of P_{2-7} show they share a common evolution. Extrapolation of these fits to

ambient pressure aligns closely with the nine distinct values between 2.1 and 2.9 cm⁻¹ (with a manifold predicted to span over 6 cm⁻¹ [1, 21]) observed via microwave absorption spectroscopy in solid para-H₂ at 1.2 K, which are assigned to reorientational transitions for pairs of J=1ortho- H_2 impurities ($nn_{ortho} = 1$). In contrast, the linear pressure dependence of the P₁ peak suggests a different origin, potentially from isolated ortho-H₂ molecules $(nn_{ortho} = 0)$ [1, 19, 21]. A similar linear pressure dependence has been reported for isolated hydrogen impurities in a solid neon matrix [33], supporting this interpretation. Furthermore, the extrapolation of the linear pressure dependence of P₁ to ambient pressure approaches that of the experimentally observed $nn_{ortho}=0$ value, 0.007 cm⁻¹ (blue circle in Fig. 4), determined through the fine structure of the infrared $Q_3(0)$ overtone $(\nu = 3 \leftarrow 0, J = 0 \leftarrow 0)$ [20].

We report low-frequency Raman excitations, below 250 cm⁻¹, in hydrogen across a broad pressuretemperature range, 2-174 GPa and 13-300 K. These peaks are interpreted as transitions among the orientational sub-levels, m_J , which are shifted from the Rayleigh line by anisotropic intermolecular interactions. These features constitute a Q_0 -branch, where the rotational quantum number J is preserved, indicating a quantum reorientational origin. This assignment is supported by the branch's behavior in phase I, which mirrors the rotational S_0 -branch under compression, as well as the subsequent quenching into phonons in phase III. At temperatures above 65 K, where samples are equilibrated with high ortho- H_2 concentration, the Q_0 -branch exhibits a Boltzmann-like distribution generated by orthopara configurational disorder and the thermal population of higher J-states. Upon cooling below 65 K, as the system approaches its equilibrium ortho-para concentration and only the J=0 and J=1 states are thermally populated, the integrated intensity of the Q_0 -branch exhibits a clear correlation with that of the $S_0(1)$ mode. This correlation strongly suggests the process originates from the m_J degeneracy of the J=1 manifold, as the non-degenerate J=0 manifold cannot contribute to this band. Finally, a fine structure is observed at low temperatures, less than 20 K, and is attributed to transitions from isolated (P_1) and ortho- H_2 pairs (P_{2-7}) . Such transitions have previously been observed only at ambient pressure [18–20]; their detection at high pressure provides a sensitive probe of the intermolecular potential in solid H₂. Our observations complete the high-pressure data set for the Raman spectrum of the archetypal coupled quantum rotor, solid hydrogen, providing new stimuli for theoretical investigations of anisotropic intermolecular interactions.

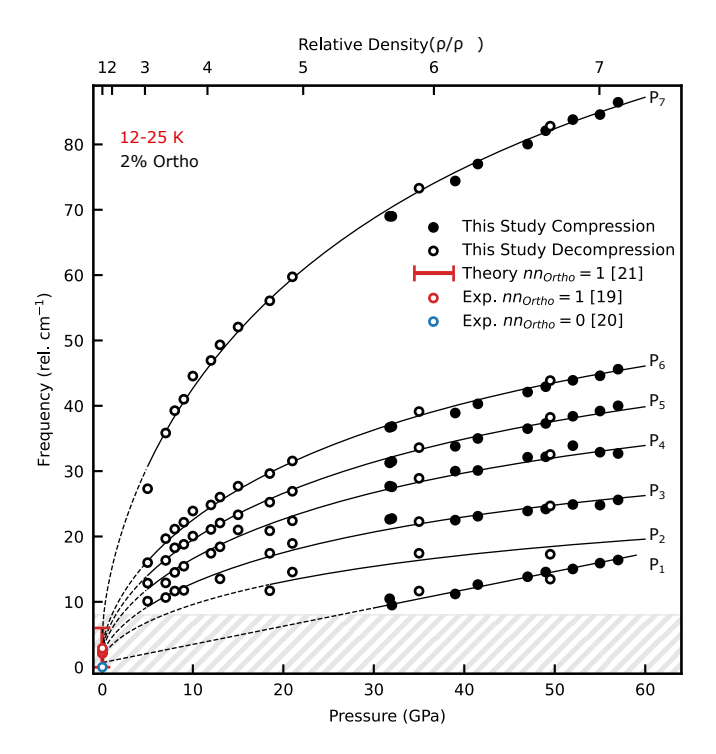


FIG. 4. Pressure dependency of low frequency excitations, P_{1-7} (denoted in Fig 3), from parahydrogen containing 2% ortho-H₂ at 13-25 K. Black solid and empty circles denote measurements carried out on compression and decompression, respectively. The solid black traces are fits to a linear function for P_1 and a global stretched exponential function for P_{2-7} (see End Matter for functional details), with extrapolations to ambient pressure shown as dashed traces. The empty red circles are taken from 9 ortho-H₂ pair excitations reported from microwave measurements on hydrogen at 1.2 K and ambient pressure [19] and the red bar represents the theoretical frequency range of the manifold [1, 34]. The empty blue circle is the experimentally determined value of an isolated ortho-H₂ molecule in parahydrogen from infrared measurements at ambient pressure and low temperatures [20]. The gray hatched region represents frequencies which are inaccessible due to the width of the notch filters used $\pm 8 \text{ cm}^{-1}$.

DATA AVAILABILITY STATEMENT

The data that support the findings of this study are available on request from the authors.

ACKNOWLEDGMENTS

P. D-S. acknowledges the support of the National Natural Science Foundation of China (NSFC) reference code W2532012. M.S. acknowledges HPSTAR for their support as a visiting scientist, during which this research was conducted.

- * philip.dalladay-simpson@hpstar.ac.cn
- † santoro@lens.unifi.it
- ‡ federico.gorelli@sharps.ac.cn
- [1] I. F. Silvera, Reviews of Modern Physics 52, 393 (1980).
- [2] J. Van Kranendonk, Solid Hydrogen (Springer New York, NY, 1983).
- [3] H. K. Mao and R. J. Hemley, Reviews of Modern Physics 66, 671 (1994).
- [4] D. M. Dennison and P. R. S. L. A, Proceedings of the Royal Society of London. Series A, Containing Papers of a Mathematical and Physical Character 115, 483 (1927).
- [5] W. Heitler and F. London, Zeitschrift für Physik 44, 455 (1927).
- [6] J. C. McLennan and J. H. McLeod, Nature 1929 123:3092 123, 160 (1929).
- [7] E. Wigner and H. B. Huntington, The Journal of Chemical Physics 3, 764 (1935).
- [8] I. F. Silvera and R. J. Wijngaarden, Physical Review Letters 47, 39 (1981).
- [9] R. J. Hemley and H. K. Mao, Physical Review Letters 61, 857 (1988).
- [10] R. T. Howie, C. L. Guillaume, T. Scheler, A. F. Goncharov, and E. Gregoryanz, Physical Review Letters 108, 125501 (2012).
- [11] P. Dalladay-Simpson, R. Howie, and E. Gregoryanz, Nature 529 (2016).
- [12] M. I. Eremets and I. A. Troyan, Nature Materials 10, 927 (2011).
- [13] L. Monacelli, M. Casula, K. Nakano, S. Sorella, and F. Mauri, Nature Physics 2023 19:6 19, 845 (2023), 2202.05740.
- [14] B. Monserrat, R. J. Needs, E. Gregoryanz, and C. J. Pickard, Physical Review B 94, 134101 (2016), 1609.07486.
- [15] N. D. Drummond, B. Monserrat, J. H. Lloyd-Williams, P. L. Ríos, C. J. Pickard, and R. J. Needs, Nature Communications 2015 6:1 6, 1 (2015).
- [16] T. Meier, D. Laniel, M. Pena-Alvarez, F. Trybel, S. Khandarkhaeva, A. Krupp, J. Jacobs, N. Dubrovinskaia, and L. Dubrovinsky, Nature Communications 11, 1 (2020).
- [17] M. Peña-Alvarez, V. Afonina, P. Dalladay-Simpson, X. D. Liu, R. T. Howie, P. I. Cooke, I. B. Magdau, G. J. Ackland, and E. Gregoryanz, Journal of Physical Chemistry Letters 11, 6626 (2020).
- [18] I. F. Silvera, W. N. Hardy, and J. P. McTague, Physical Review B 5, 1578 (1972).
- [19] W. N. Hardy and A. J. Berlinsky, Physical Review Letters 34, 1520 (1975).
- [20] R. M. Dickson, T. J. Byers, and T. Oka, Journal of Low Temperature Physics 102, 241 (1996).
- [21] W. N. Hardy, A. J. Berlinsky, and A. B. Harris, Canadian Journal of Physics 55, 1150 (1977).
- [22] P. I. Cooke, I. B. Magdău, M. Peña-Alvarez, V. Afonina, P. Dalladay-Simpson, X. D. Liu, R. T. Howie, E. Gregoryanz, and G. J. Ackland, Physical Review B 102, 1 (2020).
- [23] P. Loubeyre, R. LeToullec, D. Hausermann, M. Hanfland, R. J. Hemley, H. K. Mao, and L. W. Finger, Nature 383, 702 (1996).

- [24] Y. Akahama, Y. Mizuki, S. Nakano, N. Hirao, and Y. Ohishi, Journal of Physics: Conference Series 950, 7 (2017).
- [25] A. F. Goncharov, E. Gregoryanz, R. J. Hemley, and H.k. Mao, Proceedings of the National Academy of Sciences 98, 14234 (2001).
- [26] A. F. Goncharov, R. J. Hemley, H. kwang Mao, and J. Shu, Physical Review Letters 80, 101 (1998).
- [27] Y. Wang, X. Zhang, S. Jiang, Z. M. Geballe, T. Pakorn-chote, M. Somayazulu, V. B. Prakapenka, E. Greenberg, and A. F. Goncharov, Journal of Chemical Physics 150 (2019).
- [28] T. H. Kauffmann, N. Kokanyan, and M. D. Fontana, Journal of Raman Spectroscopy 50, 418 (2019).
- [29] P. Dalladay-Simpson, F. Capitani, and F. A. Gorelli, Physical Review B 112, 014102 (2025).
- [30] A. F. Goncharov, M. A. Strzhemechny, H. K. Mao, and R. J. Hemley, Physical Review B - Condensed Matter and Materials Physics 63, 1 (2001).
- [31] I. I. Mazin, R. J. Hemley, A. F. Goncharov, M. Hanfland, and H.-k. Mao, Physical Review Letters 78, 1066 (1997).
- [32] J. H. Eggert, E. Karmon, R. J. Hemley, H. K. Mao, and A. F. Goncharov, Proceedings of the National Academy of Sciences of the United States of America 96, 12269 (1999).
- [33] P. Loubeyre, R. Letoullec, and J. P. Pinceaux, Physical Review B 45, 12844 (1992).
- [34] A. B. Harris, A. J. Berlinsky, and W. N. Hardy, Canadian Journal of Physics 55, 1180 (1977).
- [35] G. Shen, Y. Wang, A. Dewaele, C. Wu, D. E. Fratanduono, J. Eggert, S. Klotz, K. F. Dziubek, P. Loubeyre, O. V. Fat'yanov, P. D. Asimow, T. Mashimo, and R. M. Wentzcovitch, High Pressure Research, 299 (2020).
- [36] F. Datchi, A. Dewaele, P. Loubeyre, R. Letoullec, Y. Le Godec, and B. Canny, High Pressure Research 27, 447 (2007).
- [37] Y. Akahama and H. Kawamura, Journal of Applied Physics 100 (2006), 10.1063/1.2335683/370850.
- [38] R. T. Howie, E. Gregoryanz, and A. F. Goncharov, Journal of Applied Physics 114 (2013).
- [39] W. Hayes and R. Loudon, Scattering of Light by Crystals (Wiley-Interscience, 1978).

END MATTER

Methods

For this study, we conducted a total of 6 independent experiments, using symmetric diamond anvil cells (DACs) to generate the high pressures, equipped with Type-IIas diamonds with culets 200-50 μm in diameter and a Boehler-Almax (BA) design allowing for an opening of 70°. Rhenium gaskets were prepared from 250 μ m foils by pre-indenting them to a thickness of onefifth the culet diameter and laser-machining a hole twothirds the culet size in diameter. High-purity Hydrogen (99.99% min.) was gas-loaded into the diamond anvil cell at 1.7 kbar. Throughout the experiment the applied load was generated using pressurized helium gas and a metallic-foil membrane. Pressure was primarily monitored via ruby fluorescence [35] with associated temperature corrections [36] and cross-checked using the Ramanactive phonon of the stressed diamond edge [37] and the $H_2 \text{ vibron}[38].$

Raman spectroscopy was performed utilizing a microfocused confocal optical system in a back-scattering geometry. Raman scattering was excited with 532 nm and 660 nm laser wavelengths, producing a spot size of approximately 2 μ m in diameter. To prevent excessive sample heating during measurements, the incident laser power was maintained below 5 mW. The backscattered light was collected and filtered through ultranarrow notch filters before being dispersed by a 320 mm aberration corrected spectrometer and imaged using a liquid N₂-cooled charge-coupled device detector. 1200 and 1800 gr/mm gratings were employed with exposure times of up to 10 minutes in order to reach a suitable spectral resolution and signal-to-noise ratio. Low temperature measurements were carried out using a dry cryostat using either L-N₂ or L-He as a cryogen, reaching lowest sample temperatures of 65 K and 4.5 K, respectively.

Bose-Einstein Population Correction

The raw Raman spectrum is influenced by the Bose-Einstein population factor, $n(\omega, T)$, which introduces a strong, intrinsic temperature and frequency dependence. For a phonon of vibrational frequency ω , this population number at equilibrium is given by:

$$n(\omega, T) = \frac{1}{\exp\left(\frac{\hbar\omega}{k_B T}\right) - 1}.$$
 (1)

The Stokes (I_s) and anti-Stokes (I_{aS}) intensities are proportional to $n(\omega, T) + 1$ and $n(\omega, T)$, respectively. It is important to note, that this leads to a significant intensity enhancement as $\omega \to 0$, which can strongly distort

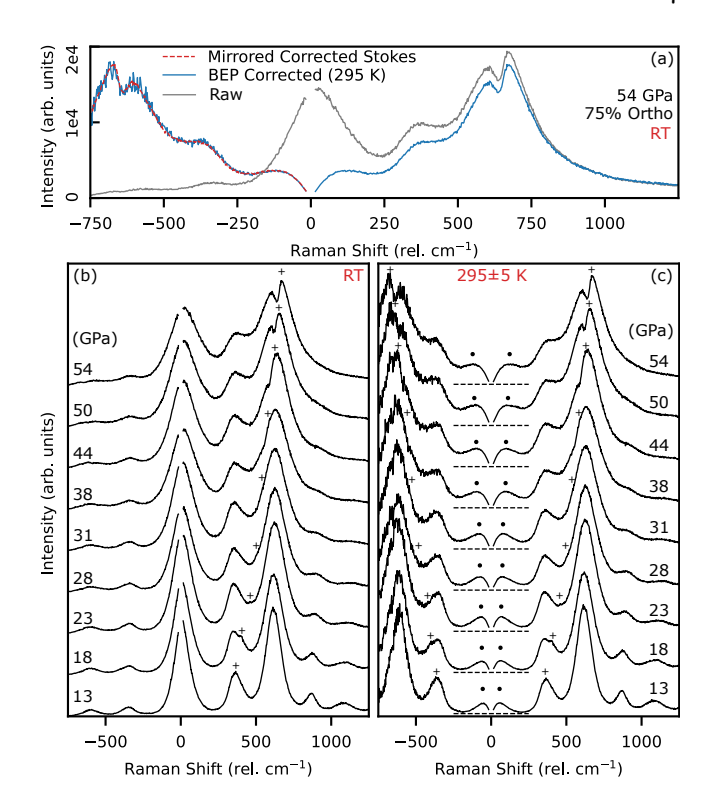


FIG. 5. Raman spectra, excited by a 660 nm laser, of solid hydrogen measured upon compression between 13-54 GPa at room temperature. (a) Raw Raman spectrum at 20 GPa (gray), the BEP corrected spectrum (blue) and the mirrored corrected Stokes spectrum (dashed red). (b) Waterfall of the raw Raman spectrum upon compression. (c) Waterfall of the BEP corrected spectra from panel (b), with the average temperature and its error bar (one SD) determined spectroscopically from the BEP corrections. Dashed horizontal lines mark the zero-intensity baselines for each spectrum. In panels (b) and (c), dots and crosses denote the maxima of the Q_0 -branch and the frequency of the E_{2g} phonon peak, respectively.

low-energy excitation lineshapes, as seen in Figs. 1(a,c), 2 and 5(a,b) between -250 cm⁻¹ and 250 cm⁻¹. Therefore, to recover the underlying Raman spectral profile, which is symmetric around zero for first-order scattering, the spectrum must be divided by this population factor. Expressing the relevant terms in Raman shift, $\Delta\nu$ (which is equal to the phonon frequency ω), this becomes the following BEP correction functions for Stokes, $\chi_S(\Delta\nu, T)$, and anti-Stokes, $\chi_{aS}(\Delta\nu, T)$ [39]:

$$\chi_S(\Delta\nu, T) \propto \frac{I_S}{(\nu_i - \Delta\nu)^3 (n(\Delta\nu, T) + 1)}$$
 (2)

$$\chi_{aS}(\Delta\nu, T) \propto \frac{I_{aS}}{(\nu_i - \Delta\nu)^3 n(\Delta\nu, T)}$$
(3)

Where $n(\Delta \nu, T) = (\exp[1.439\Delta \nu/T] - 1)^{-1}$ and $(\nu_i - \Delta \nu)^3$ relates to both fundamental electrodynamics and photoconversion in photon counting systems [39].

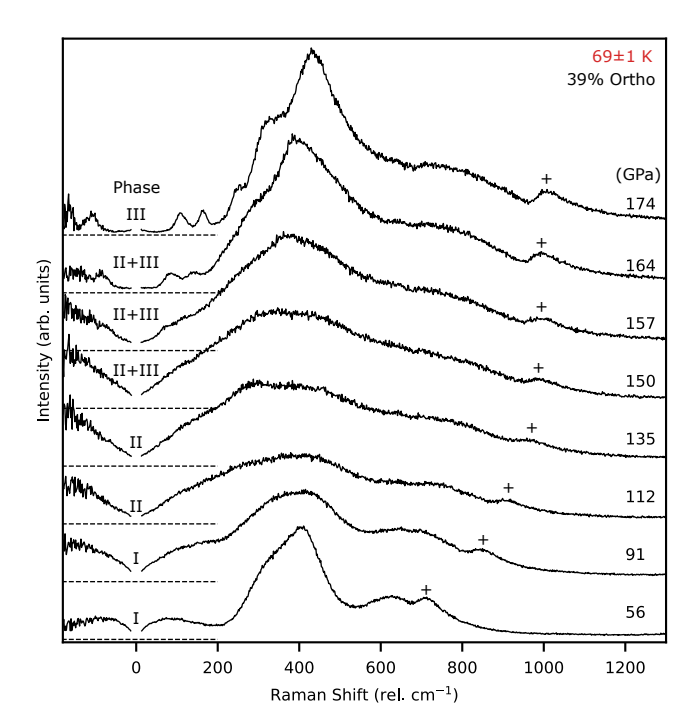


FIG. 6. Raman spectra of $\rm H_2$ at 66 K from 56-174 GPa excited by a 532 nm laser, showing the transitions between phases I, II and III. A strong phase coexistence is noted between phases II and III of approximately 25 GPa. The evolution of the E_{2g} phonon (and its equivalent mode in phases II and III [24]) is tracked by crosses. Spectral temperatures from fits during isothermal compression average 69 ± 1 K, with the error corresponding to one SD. Dashed lines indicate the zero-intensity baseline for each spectrum.

We can therefore fit a spectral temperature by minimizing the residuals between the reflected corrected Stokes and corrected anti-Stokes intensities:

$$\min_{T} f(\Delta \nu, T) = |\chi_S(-\Delta \nu, T) - \chi_{aS}(\Delta \nu, T)| \qquad (4)$$

When applied to high-quality data free from background and fluorescence, this BEP correction with a fitted temperature produces a symmetrized spectrum around the Rayleigh line. The success of this symmetrization unambiguously confirms first-order Raman scattering and yields a temperature consistent with the experimental conditions, as seen in Figs. 1, 5 and 6.

Determination of Ortho-Para Concentration

At room temperature, all hydrogen are expected to be at their equilibrium concentration of 75 % ortho-H₂.

However, at low temperatures where only the ground states of ortho- H_2 (J=1) and para- H_2 (J=0) are populated the relative ortho-concentrations, x, were determined using the integrated intensities of the rotational

TABLE I. Individual scaling factors (A_i) used in equation (6) for the global stretched-exponential fit for ortho-H₂ pair excitations (P_{2-7}) .

Excitation	A_i
P_2	0.89
P_3	1.20
P_4	1.55
P_5	1.82
P_6	2.10
P_7	3.97

 $S_0(0)$ -branch (I_0) and the $S_0(1)$ -branch (I_1) , following the formula presented by Eggert *et al.* [32] a simplified equation of what was originally proposed by Silvera *et al.* [1]:

$$x = \frac{5}{3} \left(\frac{I_0}{I_1} + \frac{5}{3} \right)^{-1} \tag{5}$$

Fitting of P_{1-7} Pressure Dependencies

The pressure dependence of the ortho- H_2 pair excitation frequencies P_{2-7} were fitted using the global stretched exponential function, equation (6).

$$\nu(P) = A_i \left(\nu_{\infty} \left(1 - \exp\left[-\left(\frac{P}{P_0} \right)^{\alpha} \right] \right) + \nu_0 \right)$$
 (6)

where A_i is an individual scaling factor for each mode (provided in Table I), while ν_{∞} (29.1 cm⁻¹), P_0 (40.6 GPa), α (0.636), and ν_0 (0.961 cm⁻¹) are shared parameters across all peaks. This functional form captures the gradual saturation of the phonon frequencies at high pressure while preserving a smooth evolution at low pressure.

The P_1 mode, suggested to be from isolated ortho- H_2 molecules, exhibited instead a distinct linear dependence and was fitted with equation (7) with the parameters $\nu_0 = 0.28~{\rm cm}^{-1}$ and $\beta = 0.71~{\rm cm}^{-1}{\rm GPa}^{-1}$.

$$\nu(P) = \nu_0 + \beta P \tag{7}$$